PCCP

ROYAL SOCIETY OF CHEMISTRY

PAPER

Cite this: *Phys. Chem. Chem. Phys.*, 2020, **22**, 5855

Microhydration of verbenone: how the chain of water molecules adapts its structure to the host molecule†

Mhamad Chrayteh, Annunziata Savoia, Thérèse R. Huet and Pascal Dréan *

Received 11th December 2019,
Accepted 13th February 2020

DOI: 10.1039/c9cp06678k

rsc.li/pccp

The microsolvation of verbenone $(C_{10}H_{14}O)\cdot(H_2O)_n$ (n = 1, 2, 3) was experimentally investigated in a supersonic expansion using a cavity-based Fourier transform microwave spectrometer, in the 2.8–14 GHz frequency range. Thanks to computationally optimized structures at the B3LYP-D3BJ/def2-TZVP and MP2/6-311++G(d,p) levels using the Gaussian 16 software, the spectra of two mono- and two dihydrates, and that of the lowest energy conformer among the four expected trihydrates, could be assigned. A similar study replacing normal water with ^{18}O labeled water allowed the identification of the spectra of all possible isotopomers, leading to the calculation of the substitution coordinates of water oxygen atoms, and of the effective structure of the water molecule arrangements around verbenone. The computed rotational constants and structural parameters were found to be quite close to the experimental ones both at the DFT and *ab initio* levels. A comparison between the structures of the hydrates of camphor previously studied by Pérez *et al.* [*J. Phys. Chem. Lett.*, 2016, **7**, 154–160] and of those of verbenone shows that the chain of water molecules adapt their structure according to the geometry of the host molecule. The general trend is that bond angles in the water chain are much wider in verbenone than in camphor.

1 Introduction

Volatile organic compounds (VOCs) are ubiquitous in the atmosphere where they are released by trees and plants.[1] Isoprene and the monoterpenes, pinenes, limonene, camphene and some of their oxygenated derivatives are the main emitted molecules. It is well established through studies in atmospheric simulation chambers or from atmospheric sampling that the oxidation of the hydrocarbons emitted by plants leads to semi-volatile organic compounds which partition into the condensed phase to form secondary organic aerosols.[2,3] Chemical reaction mechanisms are often inferred from the identification and quantification of end products.[4,5] However, what happens at a molecular level is far from understood, in particular, the role water might play in the nucleation and oxidation processes is unclear.[6–8] It could be quite important to know how water might interact with the products of oxidation, especially with monoterpenoids (bicyclic alhedydes and ketones comprising 10 atoms of carbon). Supersonic jet coupled to Fourier-transform microwave spectroscopy combined with quantum chemical calculations is a powerful technique to study the microsolvation of such molecules. The rotational spectra of monohydrates were investigated most of the time. For instance, Melandri *et al.*[9] studied the first hydrate involving a ketone, the cyclobutanone–water complex. In 2016, Pérez *et al.*[10] observed the first trihydrate of camphor, which is the first example of such a ketone surrounded by a chain of three molecules of water. The carbonyl group of ketones is the preferred site of hydration due to the available lone pairs of the oxygen atom. The chemical environment around this anchor site governs the possibility of forming the hydrates since the cohesion of the structures is also due to van der Waals interactions (or even secondary hydrogen bonds) between the oxygen atoms of the water molecules and the closest hydrogen atoms of the host molecule. It could be interesting to characterize hydrates with several monoterpenoids in order to compare their structural features and to show how the layout of the water molecules adapts to the geometry of the host molecule. We chose to study the hydrates of verbenone, which is a ketone whose rotational spectrum was recently investigated by Mashall *et al.*[11]

Verbenone ($C_{10}H_{14}O$ – 4,6,6-trimethylbicyclo[3.1.1]hept-3-en-2-one) is represented in Fig. 1, where the numbering scheme of its atoms is shown. It is a bicyclic ketone with an endocyclic

University of Lille, CNRS, UMR 8523 – PhLAM – Physique des Lasers, Atomes et Molécules, F-59000 Lille, France. E-mail: pascal.drean@univ-lille.fr; Fax: +33 3 20 33 70 20; Tel: +33 3 20 43 49 05

† Electronic supplementary information (ESI) available: Frequencies of the measured lines, experimental constants of the ^{18}O isotopic species, tables of structural parameters, SAPT0 values, NCI plots. See DOI: 10.1039/c9cp06678k

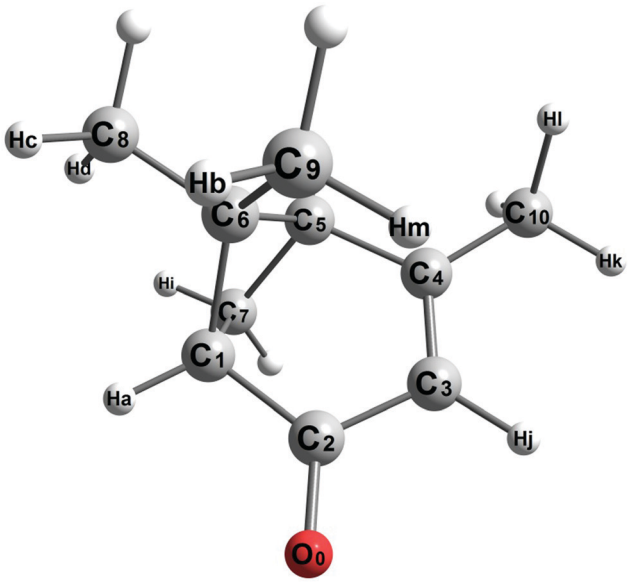

Fig. 1 Labels of the atoms of verbenone. Carbon atoms are numbered according to the official nomenclature and the hydrogen atoms involved in the formation of the hydrates with letters. The oxygen atom is numbered 0.

carbon–carbon double bond (C_3=C_4) conjugated with the carbonyl bond, which implies that the atoms C_1 to C_5, O_0 and C_{10} lie almost in the same plane (dihedral angles of $\approx 4^\circ$). The use of verbenone in chemistry takes advantage of its chirality.[12] Verbenone produced by insects, for instance bark beetles,[13] is a pheromone which can be used as semiochemicals instead of using pesticides. Verbenone was detected in samples collected in Finnish pine forests along with pinonaldehyde.[14] Their presence could be due to the photo-oxidation of α-pinene.

In this study, we present the results obtained on the hydrates of verbenone. We first present the outputs of quantum chemical calculations which prompted us to search for the experimental evidence of possible conformers. We then report on the analysis of the spectra of the hydrates and of their ^{18}O substituted isotopic species. Derivations of experimental structures were carried out and the results are compared with those obtained in the case of camphor.

2 Methods

2.1 Computational

Quantum chemical calculations were performed using Gaussian 16 Revision B.01 software[15] implemented in the computational facilities of our laboratory. The guessed structures of the hydrates were optimized using the Ahlrichs's def2-TZVP[16] basis sets at the density functional theory (DFT) B3LYP[17] level with inclusion of the D3 Grimme's dispersion scheme[18–20] with the Becke–Johnson's damping function[21–25](GD3BJ). *Ab initio* calculations were done using the Pople's 6-311++G(d,p) basis set[26–28] with diffuse and polarization functions at the second order Møller–Plesset theory (MP2)[29] level of the theory. Optimizations were conducted in the frozen-core approximation using tight convergence criteria. Harmonic frequency calculations were done to ensure that the structures corresponded to minima on the potential energy surface, to get the zero-point-energy (ZPE) corrected electronic energies and to evaluate the centrifugal distortion constants. Counterpoise corrections (basis sets superposition errors, BSSE) to the energy were calculated at the optimized geometries using the Boys–Bernardi[30] function in order to obtain the interaction energy between water and verbenone. The electrostatics, exchange, dispersion and induction terms contributing to this energy were calculated at the zeroth and second orders of symmetry adapted perturbation theory levels of the theory (SAPT0 and SAPT2)[31,32] using the truncated Dunning's basis set jun-cc-PVDZ basis set as implemented in the Psi4 program package.[33] In order to highlight the weak interactions which take place between water and verbenone, non-covalent interaction (NCI)[34] analysis was performed using the Multiwfn program[35] with input files generated with Gaussian at the MP2/6-311++G(d,p) level. Plots were made using the VMD visualization program.[36]

2.2 Experimental

The spectroscopic part of the work was performed using a cavity-based Fourier transform spectrometer already described in previous papers[37,38] working in the 2–20 GHz range. A small quantity ($\approx$0.1 mL) of verbenone (Sigma-Aldrich, (1*S*)-(−)-verbenone, 94%) used without further purification was placed in the reservoir of an injector.[39] It was heated up to 363 K (90 °C) in order to increase its vapour pressure to around 900 Pa calculated using the thermodynamic data of Štejfa *et al.*,[40] assuming that they can be extrapolated to this temperature. We noticed that it was not possible to heat it at a higher temperature without degrading it. Droplets ($\approx$0.1 mL) of normal water or ^{18}O-labeled water (Sigma-Aldrich, 97% atom ^{18}O) were introduced in a Teflon tube of 6 mm diameter and 10 cm in length connected upstream of the reservoir. The tubes and the reservoir were maintained under a pressure of 4 bars of neon, which was used as the carrier gas. A short opening (800 μs) of an orifice (Iota One, General Valve) at a repetition rate of 1 Hz enabled the gas mixture to expand into the cavity maintained under vacuum to create a supersonic jet where the rotational temperature of the molecular species was expected to be of a few Kelvins. The hydrates potentially formed in the Fanno channel and frozen in the jet were polarized by a 2 μs microwave pulse, the power of which was adjusted to get the maximum polarization (known as the π/2 condition). After a delay ranging from 10 μs to 100 μs according to the working frequency and the response of the cavity, the free induction decay was recorded using heterodyne detection to lower its frequency down to around 30 MHz. This signal was digitized by an acquisition device operating at a sampling frequency of 120 MHz. The frequency grid and hence the accuracy of the measurements were determined by the number of collected samples. When set at 65 536 or 131 072, the line positions were expected to be measured within ±2 kHz or ±1 kHz respectively. The coaxial arrangement of the two mirrors and of the jet splits each line into two Doppler components, the average of which was taken as the frequency of the transition.

3 Results

3.1 Optimized geometries

In this part, we present descriptions of the optimized structures of the hydrates. The oxygen atom of verbenone was given the number 0 as the starting point of the formation of the hydrates, and those of the water molecules were numbered from 1 to 3 depending on the hydrate we are dealing with. The hydrogen atoms of the water molecules were given numbers, while those of verbenone which play a role in the stabilization of the hydrates were labeled using small letters (Ha, Hb, *etc.*, see Fig. 1). The hydrates were named *n*w, where *n* stands for the number of water molecules, associated with a Roman numeral which designates the conformers by order of energy, starting at I for the lowest energy one.

The formation of a monohydrate is based on the establishment of a hydrogen bond between a molecule of water, which is the hydrogen donor and the oxygen atom of verbenone. We were able to optimize the structures of two monohydrates where water is attached on one side or the other of the –C═O bond. Towards the C_1 carbon, the positioning of water is governed by interactions with the water oxygen atom O_1 and the hydrogen atoms of verbenone Ha and Hb (see Fig. 2a and Fig. S2, ESI†). In conformer 1w-II (see Fig. 2b and Fig. S2, ESI†), the water molecule points towards the carbon C_3 where only the methine hydrogen atom labeled Hj is available for a secondary interaction.

Although this point is not clearly established, the formation of dihydrates is likely based on the interaction of verbenone with the water dimer, rather than a sequential addition of water to verbenone (*i.e.*, a subsequent addition of a molecule of water to the monohydrates), as already suggested by Domingos *et al.*[41] One of the water molecules of the dimer is hydrogen bonded to verbenone and the second one imposes its positioning through its interactions with the hydrogen atoms of verbenone. In the conformer 2w-I shown in Fig. 3a, the water dimer is directed to the carbon C_6 which bears the two methyl groups. The water dimer is firmly anchored to verbenone by a short hydrogen bond and by two secondary interactions between O_2 and one hydrogen atom of each methyl group. Towards the C═C carbon–carbon double bond, two very close structures of the dihydrate 2w-II differing by the orientation of the two water molecules could be optimized, referred to as 2w-II(a) as shown in Fig. 3b and 2w-II(b) which is represented in Fig. S4 (ESI†). In these two structures, the atoms C_2, O_0, O_1 and O_2 are almost coplanar.

For the trihydrate, the last molecule of the water chain can interact with verbenone far beyond the –C═O bond and the chain can distort to adapt itself to the geometry of verbenone. We were able to optimize the structure of four different conformers which are shown in Fig. S5 (ESI†). In conformers 3w-I and 3w-IV, the chain of water molecules is directed on the opposite side of the C═C double bond, respectively below and above the plane defined by the –C═O and –C═C– bonds. In conformers 3w-II and 3w-III, the chain is directed towards the C═C double bond.

3.2 Rotational spectra

The rotational spectra of the hydrates were investigated one by one, starting by the monohydrates. All the species should exhibit rather intense a-type spectra since their component of the dipole moment along the *a* axis lies in the range from 1.66 to 3.55 D. A scan showing signals related to each hydrate is presented in Fig. 4, where the intensity axis is in an arbitrary logarithmic scale. The scan shows that all the hydrates exhibit

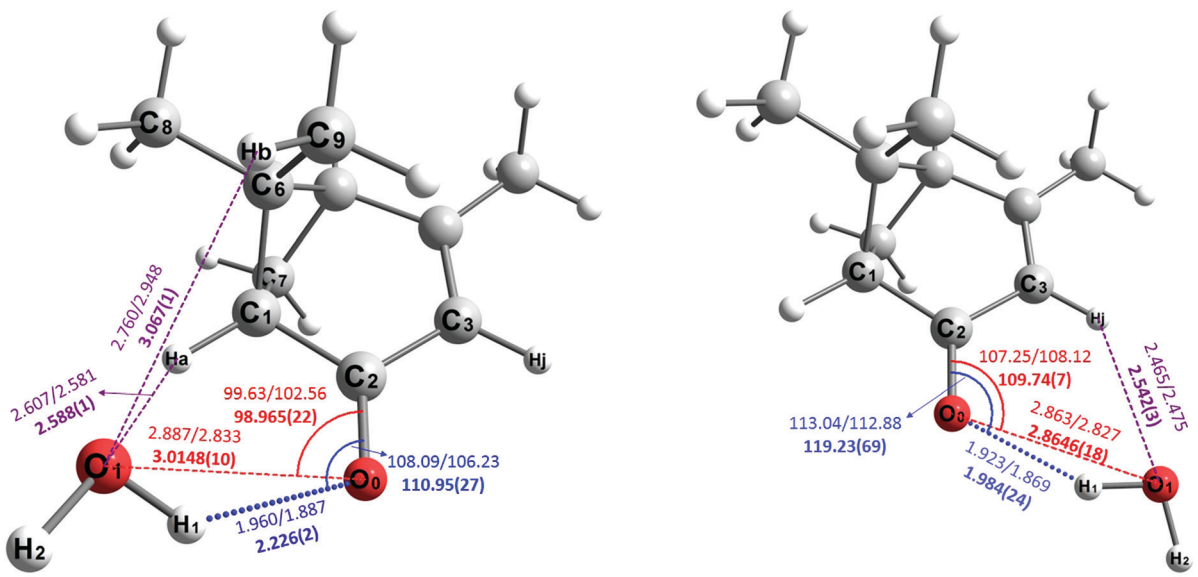

Fig. 2 The r_0 structure of the monohydrates of verbenone 1w-I and 1w-II. r_0 values are written below those of the MP2 and DFT calculations in this order. The values in red are relative to the C_2, O_0, O_1, O_2 and O_3 atoms. The values in blue are relative to the C_2, O_0 and H_1 atoms. The shortest distances between the oxygen atoms of water and hydrogen atoms of verbenone are indicated in purple. Lengths are expressed in Å and angles in °.

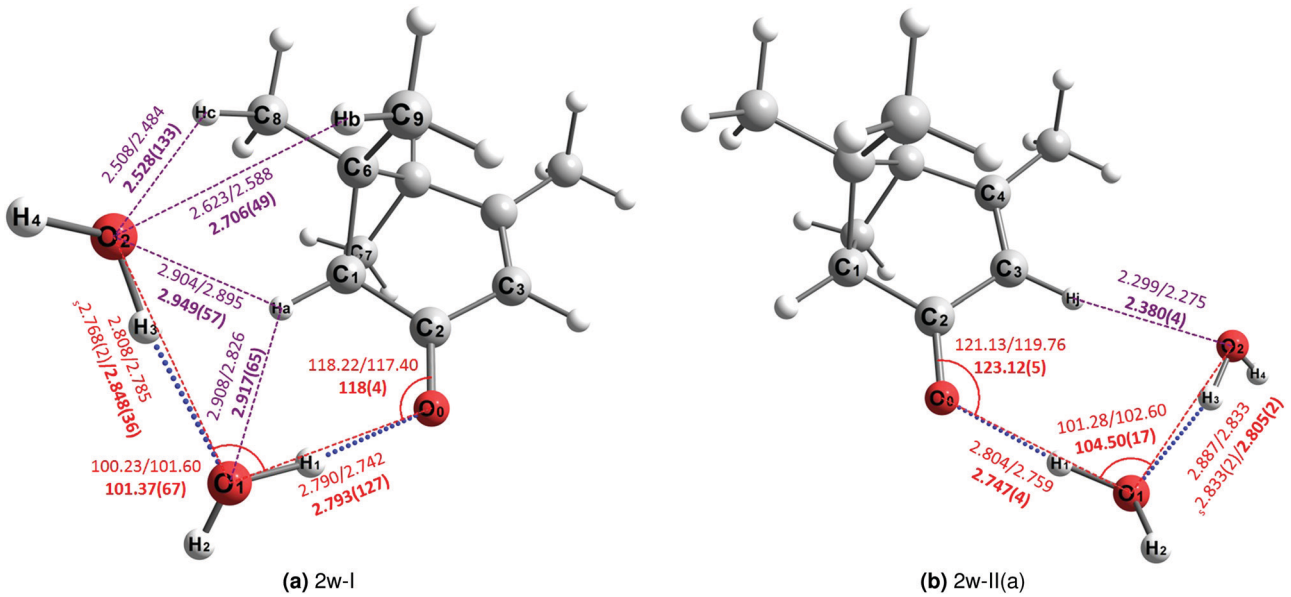

Fig. 3 The r_0 structure of the dihydrates of verbenone 2w-I and 2w-II. r_0 and the $r_s(O_1O_2)$ values are written below those of the MP2 and DFT calculations in this order. The values in red are relative to the C_2, O_0, O_1, O_2 and O_3 atoms. The shortest distances between the oxygen atoms of water and hydrogen atoms of verbenone are indicated in purple. Lengths are expressed in Å and angles in °.

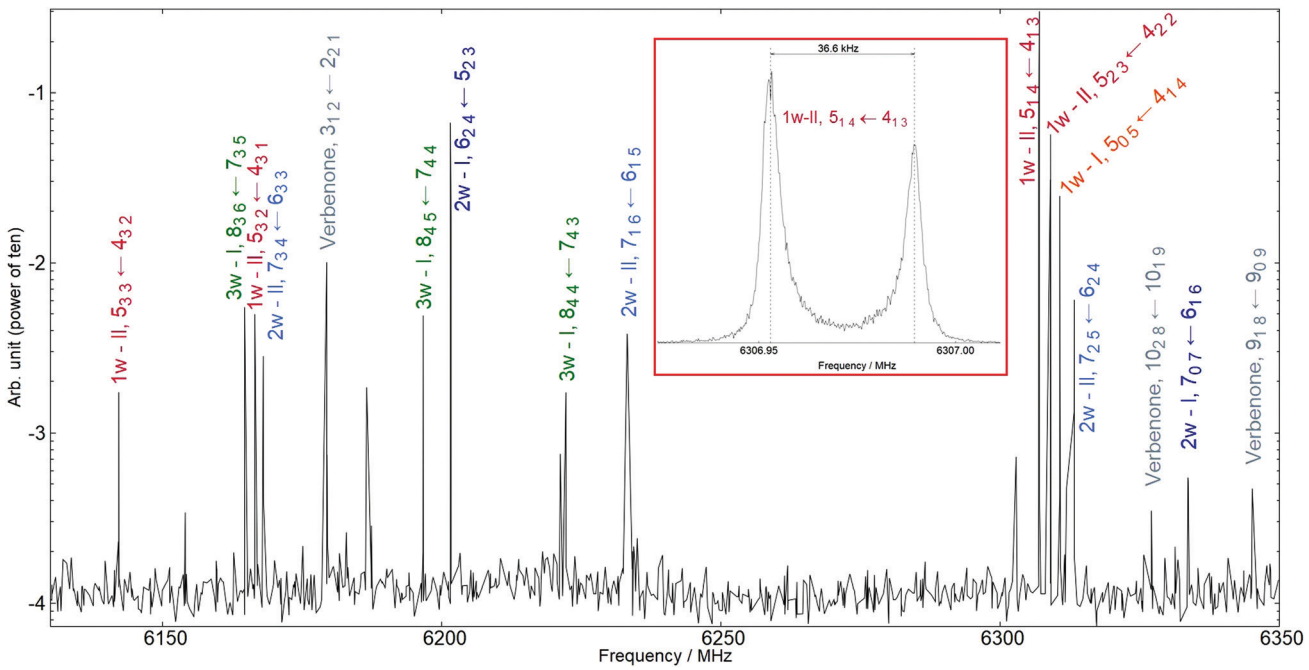

Fig. 4 A discrete scan (with a step of 250 kHz) between 6125 and 6350 MHz showing signals (each peak represents the maximum intensity in each portion of the spectra) corresponding to all the hydrates formed with normal water. Repetition rate of the nozzle: 1 Hz, number of averaged FIDs per step: 30, pulse condition set for a dipole moment of ≈2.5 D. As an example, the high resolution recording (resolution of 1 kHz, 250 acquisitions) of the $5_{14} \leftarrow 4_{13}$ line of the hydrate 1w-II showing the Doppler doubling (36.6 kHz in this case) is displayed in the panel.

lines, which clearly emerge from the noise and only a few lines remained unassigned. The starting point of the identification of each spectrum consisted in searching the $J_{0J} \leftarrow (J-1)_{0(J-1)}$ and $J_{1J} \leftarrow (J-1)_{1(J-1)}$ $^aR_{0,1}$ lines which are intense and in this case are separated by few MHz (for instance ≃13, 29 and 21 MHz for 1w-I, 2w-I and 3w-I respectively, and J = 7, see Tables S4, S14 and S32 of the ESI†). These lines could be found within 200 MHz from the predictions made using the *ab initio* rotational constants. We were able to measure from 49 to 74 lines according to the hydrate, of both a and b types, in the 2.8–14 GHz range. They are listed in Tables S4, S9, S14, S24 and S32 of the ESI.† Splittings due to a tunneling motion of the

hydrogen atoms of water were reported in some cases,[42] but it was not the case in any of the water complexes of verbenone. It could be an indication that water molecules are firmly anchored to verbenone.

The spectra of the hydrates where $H_2{}^{16}O$ was partially and totally substituted by $H_2{}^{18}O$ were also analyzed. The number of isotopic species to be studied is one for each monohydrate, three for each dihydrate and seven for the trihydrate. Lines of the isotopic species were generally found within ±2 MHz around the predictions of their frequencies calculated using constants scaled by Kisiel's COR program[43] (excepted for triple substitution, not included in the program). Once labeled water was introduced in the system, the lines of the totally substituted species could be easily measured. For the dihydrate, and even more for the trihydrate, the lines of the partially substituted species were found to be weak or even very weak, as the proportion of normal and labeled water was difficult to adjust.

All spectra could be fit to the Hamiltonian set up by Watson[44] in the A reduction, representation I^r as implemented in the CALPGM program suite (SPFIT, SPCAT) developed by Pickett.[45] The experimental constants are respectively listed in Tables 1–3 for the mono-, di- and trihydrates respectively, with the computed equilibrium rotational constants from the *ab initio* and DFT calculations and their deviations from the experimental ones. At the MP2 level, the deviations do not exceed 2%, except in the case of the monohydrate 1w-I where they reach almost 3%. Deviations from the DFT values are slightly higher. The inclusion of quartic centrifugal distortion

Table 1 Experimental rotational and quartic centrifugal constants of the two monohydrates of verbenone in the ground state, along with the equilibrium computational rotational constants and components of the dipole moment

	1w-I			1w-II		
	Exp.[a]	MP2[b,d]	DFT[c,d]	Exp.[a]	MP2[b,d]	DFT[c,d]
A/MHz	1219.96064(36)	1223.84 (0.32)	1225.37 (0.44)	1253.75046(10)	1250.21 (−0.28)	1260.99 (0.58)
B/MHz	763.38424(10)	785.38 (2.88)	781.56 (2.38)	666.514908(72)	675.90 (1.41)	676.48 (1.50)
C/MHz	608.198816(63)	626.32 (2.98)	620.78 (2.07)	554.132012(38)	560.85 (1.21)	561.99 (1.42)
Δ_J/kHz	0.26209(55)	0.095	0.147	0.09194(40)	0.092	0.084
Δ_{JK}/kHz	0.0286(26)	0.024	0.064	0.0880(26)	−0.006	0.033
Δ_K/kHz	−0.1345(48)	0.066	−0.052	—	0.209	0.119
δ_J/kHz	0.02454(20)	0.009	0.018	0.00750(21)	0.006	0.007
δ_K/kHz	0.1004(29)	0.049	0.071	−0.0693(48)	−0.075	−0.062
σ_{fit}/kHz	1.39	—	—	0.82	—	—
N_{lines}	67	—	—	68	—	—
κ^e	−0.493	−0.468 (5.07)	−0.468 (5.07)	−0.679	−0.667 (1.77)	−0.672 (0.70)
$\lvert\mu_a\rvert$/D	—	2.78	3.51	—	3.55	4.04
$\lvert\mu_b\rvert$/D	—	1.14	1.19	—	1.19	1.48
$\lvert\mu_c\rvert$/D	—	0.07	0.26	—	0.82	0.93
ΔE/kJ mol^{-1} [f]	—	0.00	0.00	—	2.02	0.64
ΔE/kJ mol^{-1} [g]	—	0.00	—	—	−0.30	—

[a] The errors in parenthesis are the standard error (confidence level 67%) in units of the last significant digits. [b] MP2/6-311++G(d,p). [c] B3LYP-D3BJ/def2-TZVP. [d] Deviation (%) calculated as (calc. − exp.)/exp. [e] $\kappa = (2B - A - C)/(A - C)$. [f] Difference in energy, including ZPE correction, with respect to the conformer 1w-I. [g] Difference in energy, including BSSE correction, with respect to the conformer 1w-I.

Table 2 Experimental rotational and quartic centrifugal constants of the two dihydrates of verbenone in the ground state, along with the equilibrium computational rotational constants and components of the dipole moment

	2w-I			2w-II(a)		
	Exp.[a]	MP2[a]	DFT[a]	Exp.[a]	MP2[a]	DFT[a]
A/MHz	1043.33007(54)	1046.00 (0.26)	1051.10 (0.74)	1063.5954(14)	1070.50 (0.65)	1071.82 (0.77)
B/MHz	546.942431(65)	550.52 (0.65)	560.08 (2.40)	473.579785(93)	471.32 (−0.48)	481.30 (1.63)
C/MHz	437.078352(28)	440.48 (0.78)	447.63 (2.41)	395.166703(58)	391.87 (−0.83)	401.60 (1.63)
Δ_J/kHz	0.04043(33)	0.033	0.031	0.08289(31)	0.046	0.060
Δ_{JK}/kHz	0.2593(22)	0.223	0.197	0.1051(26)	0.193	0.072
Δ_K/kHz	−0.202(22)	−0.171	−0.151	—	−0.096	0.058
δ_J/kHz	0.00525(16)	0.005	0.005	0.00550(22)	0.004	0.004
δ_K/kHz	0.1095(32)	0.099	0.096	0.1095(32)	0.010	−0.017
σ_{fit}/kHz	0.62	—	—	0.81	—	—
N_{lines}	74	—	—	49	—	—
κ^a	−0.637	−0.637 (0.00)	−0.627 (1.57)	−0.765	−0.765 (0.00)	−0.762 (0.39)
$\lvert\mu_a\rvert$/D	—	2.56	3.21	—	3.18	3.77
$\lvert\mu_b\rvert$/D	—	0.65	0.90	—	0.78	1.12
$\lvert\mu_c\rvert$/D	—	0.93	0.91	—	0.07	0.07
ΔE/kJ mol^{-1} [b]	—	0.00	0.00	—	4.30	3.06
ΔE/kJ mol^{-1} [b]	—	0.00	—	—	1.32	—

[a] See Table 1. [b] See Table 1, with respect to the lowest energy conformer 2w-I.

Table 3 Experimental rotational and quartic centrifugal constants of the trihydrate of verbenone 3w-I in the ground state, along with the equilibrium computational rotational constants and components of the dipole moment

	Exp.[a]	MP2[a]	DFT[a]
A/MHz	786.57406(35)	789.22 (0.34)	786.83 (0.03)
B/MHz	422.802573(55)	428.49 (1.35)	432.56 (2.31)
C/MHz	342.662068(35)	345.81 (0.92)	347.74 (1.48)
Δ_J/kHz	0.04753(15)	0.035	0.033
Δ_{JK}/kHz	0.1414(15)	0.121	0.100
Δ_K/kHz	—	0.006	0.057
δ_J/kHz	0.004 51(12)	0.003	0.005
δ_K/kHz	—	−0.009	−0.005
σ_{fit}/kHz	0.67	—	—
N_{lines}	66	—	—
κ^a	−0.639	−0.627 (1.88)	−0.614 (3.91)
$\lvert\mu_a\rvert$/D	—	1.66	2.31
$\lvert\mu_b\rvert$/D	—	0.32	0.55
$\lvert\mu_c\rvert$/D	—	0.05	0.25

[a] See Table 1.

constants was found to be necessary in order to adequately fit the spectra. A comparison shows that the calculated constants in the harmonic approximation can not be trusted, although they are in some cases in very good agreement with the experimental ones like for the dihydrate 2w-I (Table 2). We then preferred not to fix the constants at their calculated values when they could not be determined by the fit. In the fits of the spectra of the ^{18}O labeled species, the distortion constants were given the values of the parent species (or of the totally substituted species in the case of the disubstituted species of the trihydrate 3w-I). The experimental constants of the ^{18}O labeled species are given in Tables S1, S6, S11, S19 and S29 of the ESI.†

4 Structures

First of all, due to the large differences between the sets of rotational constants, each observed species present in the jet could be ascribed to a unique optimized structure, except in the case of the dihydrate 2w-II where two very close structures could be optimized. The analysis of the spectra of the isotopic species allowed us to determine the experimental structures. Partial and total substitutions of $H_2{}^{16}O$ by $H_2{}^{18}O$ yielded 3 additional constants for the monohydrate, 9 for the dihydrate and 21 for the trihydrate. The coordinates of each substituted atom of oxygen (except O_0) in the principal axes frame could be calculated using the Kraitchman's equations[46] as implemented in the KRA program written by Kisiel.[43,47] The program is fed only with experimental data (molecular mass, difference of mass upon substitution, rotational constants of the parent species and of each monosubstituted species). The error on a coordinate z is the sum of the error calculated in the KRA program propagating the errors on the rotational constants and of the error suggested by Costain:[48] $\delta z = 0.0015\ \text{Å}^2/|z|$. The method yields the absolute values of the coordinates. Their signs were inferred by comparison with those given by the quantum chemical structure optimizations.

Structures in the ground vibrational state (r_0 or effective structure) could also be derived by fitting internal coordinates (bond lengths, bond angles and dihedral angles) to all the available rotational constants of each hydrate using the Kisiel's STRFIT program.[43,47] Additional data were necessary since the number of structural parameters to be fitted was much higher than the number of rotational constants. We first assumed that the structure of verbenone was not modified upon complexation with water. Its geometry was then fixed to its r_0 structure we have recalculated using the rotational constants of verbenone and of its isotopic species obtained by Marshall *et al.*,[11] but with additional information (all those implying the hydrogen atoms) from a MP2/6-311++G(d,p) structure optimization. The effective geometry of the water molecules (r_0(O–H) = 0.965 Å and $\angle_0$(H–O–H = 104.8°)) was also fixed to that reported in ref. 49. In order to still reduce the number of structural parameters to be adjusted, all the other parameters involving the hydrogen atoms of the water molecules were taken from *ab initio* calculations in better agreement with the determined r_s structural parameters than those obtained at the DFT level. The fitted structural parameters were essentially those involving the water oxygen atoms. The position of O_1 was defined relative to the three atoms O_0, C_2 and C_3, and the position of O_2 relative to O_1, O_0 and C_2 and that of O_3 to the three previous oxygen atoms. We discuss now the structures we have determined, comparing them to those optimized by quantum chemistry and those of the hydrates of camphor.

Monohydrates

The effective structural and computationally optimized parameters we have obtained for each monohydrate are displayed in Fig. 2 for an easy comparison. The substitution coordinates of 1w-I and 1w-II (see Tables S2 and S7, ESI†) are in good agreement with the computational ones, the largest absolute deviations being 0.134 Å. Semi-experimental effective structures could be obtained, setting free four structural parameters, among them the bond angle $\angle(H_1O_1O_0)$, necessary to improve the standard deviations of the fits by one order of magnitude. The standard deviations of the fits of 0.015 μÅ^2 and 0.036 μÅ^2 for hydrates 1w-I and 1w-II respectively indicate a high-quality convergence. For conformer 1w-II, the r_0 values of the fitted parameters (see Table S8, ESI†) are consistent with the quantum chemical ones, which is not absolutely the case for 1w-I. Two fits were performed for 1w-I using as input geometry in STRFIT the DFT or the MP2 optimized position of the water molecule. The four fitted structural parameters are given in Table S3 (ESI†). The bond length $r_0(O_0O_1)$ is rather high (3.015 Å) compared to those established in the monohydrates of camphor[10] (2.857 and 2.897 Å) or in the conformer 1w-II of verbenone (2.868 Å). The bond angle $\angle(O_1O_0O_2)$ and the dihedral angle $\tau(O_1O_0C_2C_1)$ are compatible with the computed values. The value of the bond angle $\angle(H_1O_1O_0)$ is sensitive to the input value of the dihedral angle $\tau(H_2O_1H_1O_0)$ (from the MP2 or DFT calculations), converging to 29.5° or 34.0°, quite different from the calculated values of 11.4° (DFT) or 13.8° (MP2). In this case, it seems that quantum chemistry failed to correctly predict the geometry, which is corroborated by the deviations on rotational constants (see Section 3.2) and by the experimental Ray's asymmetry parameter κ of −0.493,

quite different from the calculated one of −0.468. Such deviations were also observed in the very recent study of the hydrates of acrolein.[50]

In both the conformers 1w-I and 1w-II, the second inertial moments[51] P_b and P_c of the parent and isotopic species are nearly equal (see Tables S1 and S6, ESI†). This means that the atom O_1 almost lies in the plane defined by axes *b* and *c*. This is corroborated by the small values of their coordinates along these two axes. In addition to 1w-II, the dihedral angle $\tau(O_1O_0C_2C_1)$ of 2.578° shows that the water oxygen atom is on the plane defined by the two conjugated bonds, $C_2{=}O_0$ and $C_3{=}C_4$.

Dihydrates

The experimental and computational constants and parameters of the highest energy conformer 2w-I are listed in Table 2, and those of its isotopic species with the calculated second moments of inertia in Table S11 (ESI†). The substitution coordinates of the atoms O_1 and O_2 along with those given by the optimizations are given in Table S12 (ESI†). They are in very good agreement, except for the value of the coordinate of O_1 along the *c* axis, but as it is small, it should be considered with caution. To determine the effective structure, five structural parameters listed in Table S13 (ESI†) were fitted to the twelve moments of inertia. The $r_0(O_1O_2)$ bond length (2.842 Å) is in very close agreement with its r_s value (2.848 Å). The bond angles $\angle(O_1O_0C_2)$ and $\angle(O_2O_1O_0)$, and the dihedral angle $\tau(O_2O_1O_0C_2)$ were well predicted by computational chemistry with deviations which do not exceed 1°. The structure of the dihydrate 2w-I is likely to be reliable.

Two close structures of the highest energy conformer 2w-II were optimized (see Section 3.1). The difference of electronic energy between the two structures, including ZPE correction is 0.2 kJ mol^{-1} at the MP2/6-311++G(d,p) level, which is not significant. If each conformer had given rise to its own spectrum, lines of about the same intensity separated by a few MHz should have been observed, which is not the case. Deviations between calculated (MP2/6-311++G(d,p)) and experimental rotational constants were found to be a bit smaller in the case of conformer 2w-II(a) (−0.8 to +0.7%), compared to the case of conformer 2w-II(b) (+1.1 to +1.4%). This comparison carried out between equilibrium and effective constants is not conclusive since they are nevertheless of the same order of magnitude. Comparison with the coordinates taken from the MP2/6-311++G(d,p) optimizations (see Tables S20 and S22, ESI†) shows that they match structure 2w-II(a) slightly better, but it is still hard to conclude that it is this conformer that was observed in the jet. Effective structures were also calculated. Two fits were performed. Using the geometry of conformer 2w-II(b) as the starting point, we found that it was necessary to set free the dihedral angle $\tau(H_4O_2H_3O_1)$, which converged to a value far from those predicted by quantum chemical calculations (see Table S23, ESI†). When the geometry of the dihydrate 2w-II(a) was used, the five parameters defining the position of the two water oxygen atoms could be adjusted. They converged to values compatible with those calculated. Although the arguments are tenuous, they all indicate that the conformer 2w-II(a) is likely to be observed in the jet. The use of deuterated water could have been useful as a definitive proof. It is known that substitution of a hydrogen atom with a deuterium deeply affects the molecular structure, especially when they are involved in a hydrogen bond. In their study on the cyclobutanone–water complex, Melandri *et al.*[9] showed that the use of deuterated water led to data that was hard to use. We therefore did not try to perform experiments with deuterium.

Trihydrate 3w-I

The rotational constants of the trihydrate monosubstituted in each position were used to calculate the substitution coordinates of the three water oxygen atoms presented in Table S30 (ESI†). There is a very good agreement between the experimental and computational coordinates, except when they have small values, which mainly occur along the *c* principal axis. In this case, the reliability of the r_s coordinates may be questioned. The positions of the three atoms of oxygen are then likely to be reliable. Nevertheless, the deviation between the experimental and calculated Ray's asymmetry parameter of the trihydrate 3w-I is rather high, 1.9% and 3.9%, considering the MP2 and DFT values respectively (Table 3). This may be due to inexact positions of the hydrogen atoms of water. It was not possible to set free some structural parameters involving these atoms in the fit of a semi-experimental effective structure. The three bond lengths $r(O_0{-}O_1)$, $r(O_1{-}O_2)$, $r(O_2{-}O_3)$ and the dihedral angles $\tau(O_2O_1O_0C_2)$ and $\tau(O_3O_2O_1O_0)$ were fitted. Their output values are listed in Table S31 (ESI†) and the structural data of the trihydrate 3w-I are graphically summarized in Fig. 5. The bond lengths $r(O_1{-}O_2)$ and $r(O_2{-}O_3)$ can be compared with those calculated using the r_s coordinates. They are in agreement within their uncertainties. The two adjusted dihedral angles take values close to the *ab initio* ones.

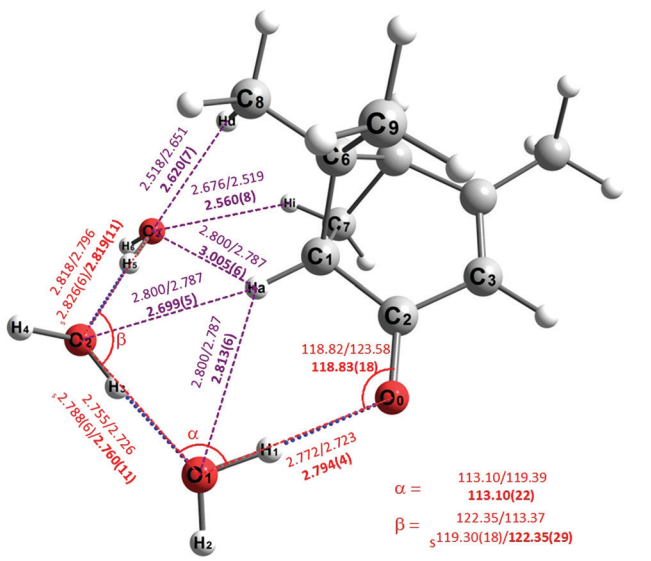

Fig. 5 The r_0 structure of the trihydrate of verbenone 3w-I. r_0 values, the $r_s(O_1O_2)$ and $r_s(O_2O_3)$ values are written below those of the MP2 and DFT calculations in this order. The values in red are relative to the C_2, O_0, O_1, O_2 and O_3 atoms. The shortest distances between oxygen atoms of water and hydrogen atoms of verbenone are indicated in purple. Lengths are expressed in Å and angles in °.

Comparison of structures

The structures of the hydrates of verbenone can be compared to those obtained in the case of camphor.[10] The general trend is that the bond angles in the chain of water molecules are wider in the case of verbenone. For instance, the $\angle_0(O_0O_1O_2)$ values are 82.17° and 89.17° in the two dihydrates of camphor, and 101.37° and 104.50° in those of verbenone. Some structural parameters of the trihydrates of verbenone and camphor are listed in Table 5. Again, the main differences concern the bond angles. The angle connecting O_1, O_2 and O_3 (named β in Fig. 5) is 122.35° in the trihydrate of verbenone and 103.44° in that of camphor. To explain these large differences, we can invoke the presence of the two hydrogen atoms, Ha and Hj (Fig. 3 and 5) which exert a repulsion on the hydrogen-bonded water hydrogen atoms. Indeed, the NCI plots depicted in Fig. S6 (ESI†) and nci, shows that the isosurface is composed of green parts (weak attractive interactions) and brown-orange parts (weak repulsive interactions). In particular, the NCI plot of the trihydrate of verbenone shown in Fig. 6a reveals that the three water oxygen atoms establish weak attractive interactions with the hydrogen atom Ha while there are weak repulsions between the hydrogen atoms of water H_1, H_3 and H_5, at the origin of a more opened structure. In verbenone, the three molecules of water seem to wrap around verbenone, while in camphor they are away from the host molecule. We can also state that in camphor, the last oxygen atom of the water chain interacts with hydrogen atoms located at distances of 2.837 Å and 4.237 Å from the oxygen atom of the carbonyl moiety, while in verbenone the distances are 4.339 Å and 5.111 Å. It also explains that the chain closes on itself in camphor, in order to reach the hydrogen atoms. Finally, the dihedral angle $\tau(O_0O_1O_2O_3)$ is larger in verbenone than in camphor, which shows that the arrangement is not necessarily close to planarity.

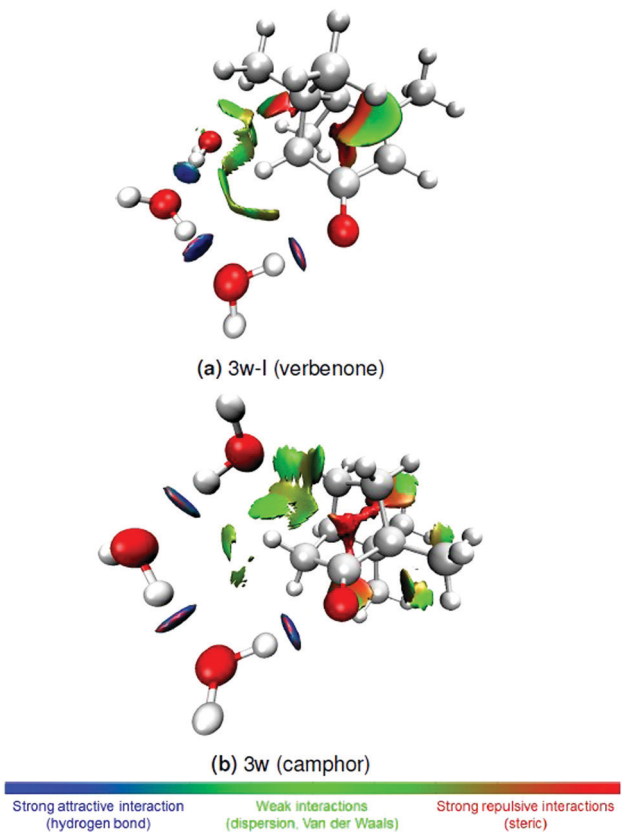

Fig. 6 NCI plots showing the interactions in the trihydrates of verbenone and camphor.

SAPT and BSSE calculations

The contributions of the electrostatics, exchange, induction and dispersion to the total interaction energy for the monohydrates and the dihydrates at the SAPT2 level are given in Table 4 (those at the SAPT0 level are listed in Table S40, ESI†). Two fragments were considered in the calculations: verbenone and the chain of water molecules. According to these results, the main contribution to the cohesion of the hydrates is due to the electrostatic part mainly related to the –C=O···H–O hydrogen bond, with values slightly higher than −50 kJ mol^{-1} and −70 kJ mol^{-1}, respectively, for monohydrates and dihydrates. The hydrogen bond is then much stronger in the latter case which is the reflection of hydrogen bond cooperation. While the values are very close for the dihydrates, there is a difference of 4.84 kJ mol^{-1} between 1w-I and 1w-II, which corroborates the longer hydrogen bond determined in 1w-I (see Fig. 2). Dispersion mainly due to the weak interactions between water oxygen atoms and verbenone hydrogen atoms also contribute to the cohesion of the structures in a non-negligible way, with values ranging from −11.30 to −19.15 kJ mol^{-1}. The higher absolute value of the dispersion energy in 1w-I partly compensates for the relative weakness of the hydrogen bond. For dihydrates, there is a large difference between dispersion energies of 3.63 kJ mol^{-1} in favor of 2w-I. This is particularly striking in the NCI plots (see Fig. S6, ESI†), with a wide isosurface in 2w-I due to multiple interactions compared with 2w-II(a). Complexation energies (two last columns of Table 4) obtained from the SAPT2 and counterpoise calculations are in fair agreement, except for 3w-I which could be due to the geometry of the fragment made of three molecules of water known to be cyclic[52] in an isolated environment, but which adopts a very different geometry in the complex. They increase from the mono- to the trihydrate, which is due both to stronger hydrogen bonds and higher absolute dispersion energies. It should be mentioned that 1w-I is the lowest energy conformer considering the ZPE corrected energy by 2.02 kJ mol^{-1}, but the highest energy one considering the

Table 4 Decomposition of the interaction energy between verbenone and water as calculated at the SAPT2/jun-cc-PVDZ level of theory, values in kJ mol^{-1}, and BSSE corrected interaction energies at the MP2/6-311++G(d,p) level

	E_{elec}	E_{exch}	E_{ind}	E_{disp}	E_{SAPT2}	E_{BSSE}
1w-I	−43.87	47.84	−14.82	−13.61	−24.47	−25.22
1w-II	−48.71	51.41	−16.01	−11.30	−24.61	−25.61
2w-I	−69.16	75.11	−27.72	−19.15	−40.92	−42.17
2w-II(a)	−68.30	70.31	−26.14	−15.52	−39.65	−40.71
3w-I	−93.89	77.55	−36.65	−22.65	−75.64	−50.28

Table 5 Comparison of effective structural parameters of the trihydrates of verbenone and camphor (from the data of Pérez *et al.*[10])

Parameter[a]	3w-I verbenone	3w camphor
$r(O_0–O_1)$/Å	2.794(34)	2.804(5)
$r(O_1–O_2)$/Å	2.760(11)	2.761(3)
$r(O_2–O_3)$/Å	2.819(11)	2.800(3)
$r(O_0\cdots H_1)$/Å	1.831(8)	1.84(1)
$r(O_1\cdots H_3)$/Å	1.798(7)	1.81(1)
$r(O_2\cdots H_5)$/Å	1.854(8)	1.84(1)
$r(O_3–H_d)$/Å	2.620(7)	2.592(16)
$r(O_3–H_i)$/Å	2.560(8)	2.518(14)
$\angle(C_2–O_0–O_1)$/°	118.83(18)	114.97(24)
$\angle(O_0–O_1–O_2)$/°	113.10(22)	100.59(13)
$\angle(O_1–O_2–O_3)$/°	122.35(29)	103.44(8)
$\tau(O_0–O_1–O_2–O_3)$/°	24.73(73)	10.51(22)

[a] The labels of the atoms are those indicated in Fig. 5 for verbenone and may not correspond to the labeling chosen for camphor.

counterpoise corrected energy, with a difference of 0.30 kJ mol^{-1}. The SAPT2 complexation energies confirm this fact, but they are calculated with errors of $\approx$0.5 kJ mol^{-1},[32] higher than the difference of energy between 1w-I and 1w-II. We can hence not conclude which of 1w-I and 1w-II is the lowest energy conformer.

Regarding the trihydrates, in 3w-I, the atoms of oxygen of water O_1 and O_2 interact with hydrogen atoms of verbenone Ha, Hi, and Hc at distances lower than 2.800 Å, which is not the case in conformers 3w-II to 3w-IV with the smallest distance being 3.095 Å in 3w-III. The comparison of the NCI plots (see Fig. S7, ESI†) shows that the interactions are the weakest in conformers 3w-II and 3w-IV and the strongest in conformers 3w-I and 3w-III. The dihedral angle $\tau(O_0O_1O_2O_3)$ also plays a role in the ordering of the energies. A high value disadvantages the cooperativity between hydrogen bonds and increases the energy. Absolute values of 47.3° and 29.5° in 3w-III and 3w-IV (Fig. S5, ESI†) are indeed related to the highest energy conformers.

5 Conclusions

In this study, the complexes of verbenone with water, up to the trihydrates, were characterized using quantum chemical calculations and microwave Fourier transform spectroscopy. The structure of two mono-, three di- and four trihydrates were optimized at the B3LYP-D3BJ/def2-TZVP and MP2/6-311++G(d,p) levels. They consist in a single molecule of water, a water dimer or an open water trimer attached to verbenone by a strong hydrogen bond –C═O–H–O and mainly interacting with the hydrogen atoms of the two methyl groups and with the methine hydrogen on each side of the carbonyl bond. We were able to analyse the spectra of the two monohydrates, of two dihydrates and of the lowest energy conformer of the four predicted trihydrates. In order to determine experimentally the layout of the molecules of water around verbenone, the spectra of the hydrates where normal water was partially and totally substituted by ^{18}O labeled water were analyzed. Substitution coordinates of the oxygen atoms were obtained using Kraitchman's equations. Both DFT and *ab initio* methods were able to correctly predict the position of the water oxygen atoms, but not necessarily the orientation of the water molecules. Semi-experimental effective structures were also derived by fitting structural parameters to all the available moments of inertia of each hydrate. Our study showed in particular that the chain of three water molecules adopts an opened structure. The characterization of the isotopic species where the oxygen atom of the host molecule is itself substituted may also be of great help to get even more reliable experimental structures. The observation of the highest energy conformers of the trihydrates, as well as the observation of even more solvated verbenone, is also a challenging task.

Conflicts of interest

There are no conflicts to declare.

Acknowledgements

The present work was funded by the French ANR Labex CaPPA through the PIA under contract ANR-11-LABX-0005-01, by the Regional Council Hauts de France, by the European Funds for Regional Economic Development (FEDER), and by the French Ministère de l'Enseignement Supérieur et de la Recherche. It is a contribution to the CPER research Project CLIMIBIO. F. Réal is deeply acknowledged for the SAPT calculations, for helpful discussions and for the corrections of the manuscript.

Notes and references

1 S. Moukhtar, C. Couret, L. Rouil and V. Simon, *Sci. Total Environ.*, 2006, **354**, 232–245.
2 U. Baltensperger, M. Kalberer, J. Dommen, D. Paulsen, M. Alfarra, H. Coe, R. Fisseha, A. Gascho, M. Gysel, S. Nyeki, M. Sax, M. Steinbacher, A. Prevot, S. Sjögren, E. Weingartner and R. Zenobi, *Faraday Discuss.*, 2005, **130**, 265–278.
3 A. Mutzel, M. Rodigast, Y. Iinuma, O. Böge and H. Herrmann, *Atmos. Environ.*, 2016, **130**, 136–144.
4 V. Librando and G. Tringali, *J. Man. Environ.*, 2005, **75**, 275–282.
5 T. Hohaus, I. Gensch, J. Kimmel, D. Worsnop and A. Kiendler-Scharr, *Phys. Chem. Chem. Phys.*, 2015, **17**, 14796–14804.
6 L. Stirnweis, C. Marcolli, J. Dommen, P. Barmet, C. Frege, S. Platt, E. Bruns, M. Krapf, J. Slowik, R. Wolf, A. Prévôt, U. Baltensperger and I. El-Haddad, *Atmos. Chem. Phys.*, 2017, **17**, 5035–5061.
7 S. Sarkar, Monu and B. Bandyopadhyay, *Atmos. Environ.*, 2019, **213**, 223–230.
8 V. Vaida, *J. Chem. Phys.*, 2011, **135**, 020901.
9 S. Melandri, A. Maris, B. Giuliano and W. Caminati, *J. Chem. Phys.*, 2005, **123**, 164304.
10 C. Pérez, A. Krin, A. Steber, J. López, Z. Kisiel and M. Schnell, *J. Phys. Chem. Lett.*, 2016, **7**, 154–160.
11 F. Marshall, G. Sedo, C. West, B. Pate, S. Allpress, C. Evans, P. Godfrey, D. McNaughton and G. S. Grubbs II, *J. Mol. Spectrosc.*, 2017, **342**, 109–115.
12 Z. Rafiński and M. Krzemiński, *Catalysts*, 2019, **9**, 117.

13 C. Gitau, R. Bashford, A. Carnegie and G. Gurr, *For. Ecol. Manage.*, 2013, **297**, 1–14.
14 T. Rissanen, T. Hyötyläinen, M. Kallio, J. Kronholm, M. Kulmala and M.-L. Riekkola, *Chemosphere*, 2006, **64**, 1185–1195.
15 M. J. Frisch, G. W. Trucks, H. B. Schlegel, G. E. Scuseria, M. A. Robb, J. R. Cheeseman, G. Scalmani, V. Barone, G. A. Petersson, H. Nakatsuji, X. Li, M. Caricato, A. V. Marenich, J. Bloino, B. G. Janesko, R. Gomperts, B. Mennucci, H. P. Hratchian, J. V. Ortiz, A. F. Izmaylov, J. L. Sonnenberg, D. Williams-Young, F. Ding, F. Lipparini, F. Egidi, J. Goings, B. Peng, A. Petrone, T. Henderson, D. Ranasinghe, V. G. Zakrzewski, J. Gao, N. Rega, G. Zheng, W. Liang, M. Hada, M. Ehara, K. Toyota, R. Fukuda, J. Hasegawa, M. Ishida, T. Nakajima, Y. Honda, O. Kitao, H. Nakai, T. Vreven, K. Throssell, J. A. Montgomery, Jr., J. E. Peralta, F. Ogliaro, M. J. Bearpark, J. J. Heyd, E. N. Brothers, K. N. Kudin, V. N. Staroverov, T. A. Keith, R. Kobayashi, J. Normand, K. Raghavachari, A. P. Rendell, J. C. Burant, S. S. Iyengar, J. Tomasi, M. Cossi, J. M. Millam, M. Klene, C. Adamo, R. Cammi, J. W. Ochterski, R. L. Martin, K. Morokuma, O. Farkas, J. B. Foresman and D. J. Fox, *Gaussian 16, Revision B.01*, Gaussian Inc., Wallingford CT, 2016.
16 F. Weigend and R. Ahlrichs, *Phys. Chem. Chem. Phys.*, 2005, **7**, 3297–3305.
17 P. Stephens, F. Devlin, C. Chabalowski and M. Frisch, *J. Phys. Chem.*, 1994, **98**, 11623–11627.
18 S. Grimme, *J. Comput. Chem.*, 2004, **25**, 1463–1473.
19 S. Grimme, J. Antony, S. Ehrlich and H. Krieg, *J. Chem. Phys.*, 2010, **132**, 154104.
20 S. Grimme, *Wiley Interdiscip. Rev.: Comput. Mol. Sci.*, 2011, **1**, 211–228.
21 A. Becke, *Phys. Rev. A: At., Mol., Opt. Phys.*, 1988, **38**, 3098–3100.
22 A. Becke, *J. Chem. Phys.*, 1993, **98**, 5648–5652.
23 A. Becke and E. Johnson, *J. Chem. Phys.*, 2005, **123**, 154101.
24 E. Johnson and A. Becke, *J. Chem. Phys.*, 2005, **123**, 024101.
25 E. Johnson and A. Becke, *J. Chem. Phys.*, 2006, **124**, 174104.
26 W. Hehre, K. Ditchfield and J. Pople, *J. Chem. Phys.*, 1972, **56**, 2257–2261.
27 R. Krishnan, J. Binkley, R. Seeger and J. Pople, *J. Chem. Phys.*, 1980, **72**, 650–654.
28 M. Frisch, J. Pople and J. Binkley, *J. Chem. Phys.*, 1984, **80**, 3265–3269.
29 C. Møller and M. S. Plesset, *Phys. Rev.*, 1934, **46**, 618–622.
30 S. Boys and F. Bernardi, *Mol. Phys.*, 1970, **19**, 553–566.
31 B. Jeziorski, R. Moszynski and K. Szalewicz, *Chem. Rev.*, 1994, **94**, 1887–1930.
32 T. Parker, L. Burns, R. Parrish, A. Ryno and C. Sherrill, *J. Chem. Phys.*, 2014, **140**, 094106.
33 R. Parrish, L. Burns, D. Smith, A. Simmonett, A. DePrince, E. Hohenstein, U. Bozkaya, A. Sokolov, R. Di Remigio, R. Richard, J. Gonthier, A. James, H. McAlexander, A. Kumar, M. Saitow, X. Wang, B. Pritchard, P. Verma, H. Schaefer, K. Patkowski, R. King, E. Valeev, F. Evangelista, J. Turney, T. Crawford and C. Sherrill, *J. Chem. Theory Comput.*, 2017, **13**, 3185–3197.
34 E. Johnson, S. Keinan, P. Mori-Sánchez, J. Contreras-García, A. Cohen and W. Yang, *J. Am. Chem. Soc.*, 2010, **132**, 6498–6506.
35 T. Lu and F. Chen, *J. Comput. Chem.*, 2012, **33**, 580–592.
36 W. Humphrey, A. Dalke and K. Schulten, *J. Mol. Graphics*, 1996, **14**, 33–38.
37 M. Tudorie, L. H. Coudert, T. R. Huet, D. Jegouso and G. Sedes, *J. Chem. Phys.*, 2011, **134**, 074314.
38 M. Chrayteh, P. Dréan and T. Huet, *J. Mol. Spectrosc.*, 2017, **336**, 22–28.
39 S. Kassi, D. Petitprez and G. Wlodarczak, *J. Mol. Spectrosc.*, 2004, **228**, 293–297.
40 V. Štejfa, M. Fulem, K. Ružička, C. Červinka, M. Rocha, L. Santos and B. Schröder, *J. Chem. Thermodyn.*, 2013, **60**, 117–125.
41 S. R. Domingos, C. Pérez and M. Schnell, *J. Chem. Phys.*, 2016, **145**, 161103.
42 W. Huang, J. Thomas, W. Jäger and Y. Xu, *Phys. Chem. Chem. Phys.*, 2017, **19**, 12221–12228.
43 Z. Kisiel, PROSPE – Programs for ROtational SPEctroscopy, http://www.ifpan.edu.pl/kisiel/prospe.htm, accessed: 2017-02-14.
44 J. Watson, *Mol. Phys.*, 1968, **15**, 479–490.
45 H. M. Pickett, *J. Mol. Spectrosc.*, 1991, **148**, 371–377.
46 J. Kraitchman, *Am. J. Phys.*, 1953, **21**, 17–24.
47 Z. Kisiel, in *Spectroscopy from Space*, ed. J. Demaison, K. Sarka and E. A. Cohen, Kluwer Academic Publishers, Dordrecht, 2001, pp. 91–106.
48 C. C. Costain, *Trans. Am. Crystallogr. Assoc.*, 1966, **21**, 157–164.
49 M. Harmony, V. Laurie, R. Kuczkowski, R. Schwendeman, D. Ramsay, F. Lovas, W. Lafferty and A. Maki, *J. Chem. Phys. Ref. Data*, 1979, **8**, 619–722.
50 W. Li, A. Maris, C. Calabrese, I. Usabiaga, W. D. Geppert, L. Evangelisti and S. Melandri, *Phys. Chem. Chem. Phys.*, 2019, **21**, 23559–23566.
51 R. K. Bohn, J. A. Montgomery, H. H. Michels and J. A. Fournier, *J. Mol. Spectrosc.*, 2016, **325**, 42–49.
52 F. Keutsch, J. Cruzan and R. Saykally, *Chem. Rev.*, 2003, **103**, 2533–2577.

